Carbohydrate Polymers 179 (2018) 79–85

Contents lists available at ScienceDirect

Carbohydrate Polymers

journal homepage: www.elsevier.com/locate/carbpol

Research Paper

Combined effect of cellulose nanocrystals and poly(butylene succinate) on poly(lactic acid) crystallization: The role of interfacial affinity

Xiaocan Zhang[a,b,*], Jiafeng Shi[b,c], Haimu Ye[a,b], Yuhua Dong[a,b], Qiong Zhou[a,b]

[a] State Key Laboratory of Heavy Oil Processing, China University of Petroleum, Beijing 102249, China
[b] College of Science, China University of Petroleum, Beijing 102249, China
[c] CNPC Research Institute of Engineering Technology, Tianjin 300451, China

ARTICLE INFO

Keywords:
Cellulose nanocrystal
Poly(lactic acid)
Poly(butylene succinate)
Composite
Interfacial affinity

ABSTRACT

Poly (lactic acid) (PLA)/cellulose nanocrystals (CNC), poly(butylene succinate) (PBS)/CNC and PLA/PBS/CNC composite films were prepared using a solution-casting technique. CNCs can be used to enhance the crystallization of PLA by offering more nucleation sites, and PBS can increase spherulite growth rate of PLA by providing flexible chains. However, CNCs and PBS together tend to interfere with each other and thus enhancement in the crystallization of PLA is lost. FTIR, contact-angle measurements, and dissolution experiments were used to characterize the materials. It was found that the interfacial affinity was greater in the CNC–PBS system than the CNC–PLA system. It was therefore concluded that the PBS chains occupy most of the CNC surfaces in the molten state before cooling. Consequently, PLA was mainly blocked from the CNCs and the nucleation effect was greatly weakened. The binary and ternary composite systems are discussed in terms of their crystallization processes.

1. Introduction

Poly(lactic acid) (PLA), derived from renewable resources, has always received considerable attention in the search for sustainable and environmentally friendly materials (Chen & Patel, 2011). It is an aliphatic thermoplastic polyester with high modulus, high strength and good clarity. However, the poor toughness and relatively slow crystallization rate are the main disadvantages that restrict its wider application (Auras, Harte, & Selke, 2004; Saeidlou, Huneault, Li, & Park, 2012; Sinba, 2012).

In order to achieve desired mechanical properties without compromising its biodegradability, PLA can be blended with a plasticizer such as poly(butylene succinate) (PBS). PBS is an attractive material with environmental and ecological advantages. It is flexible and tough, and blending PLA with PBS has generated great interest from many research groups (Park & Im, 2002; Park, Hwang, Moon, Im, & Yoo, 2010; Shibata, Inoue, & Miyoshi, 2006; Yokohara & Yamaguchi, 2008; Zhang, Liu, Shi, Ye, & Zhou, 2017). The addition of PBS has been reported to accelerate the spherulite growth rate of PLA. Nanoparticles are also good nucleation agents (Harris & Lee, 2008; Pan & Qiu, 2010; Ye, Hou, & Zhou, 2016; Yu, Liu, Zhao, Lu & Wang, 2012), and they can enhance the nucleation ability of a polymer matrix, exhibiting increased nucleation sites and crystallization rates (Zhao & Qiu, 2015).

Cellulose nanocrystals (CNC) have received increasing attention as they have unique morphology, low density, and high mechanical strength, and because they are renewable and biodegradable (Habibi, Lucia, & Rojas, 2010). CNC can be derived from cellulose, which is one of the most abundant substances in nature. Subsequently, CNCs can be used as a 'green' nucleation agent as well as a source for polymer reinforcements, which is essential to enhance the mechanical properties of the composite. Numerous researchers (Barrau et al., 2011; Kamal & Khoshkava, 2015; Lin, Huang, Chang, Feng, & Yu, 2011; Lizundia, Vilas, & León, 2015; Lizundia et al., 2016; Luzi et al., 2016) have doped PLA with CNCs and a resultant increase in the crystallization rate as well as an enhancement in the mechanical properties were generally found.

CNCs have also been reported to reinforce PBS by serving as additional nucleation sites (Hu, Lin, Chang, & Huang, 2015; Lin, Chen, Hu, & Huang, 2015). Therefore, it would be interesting to see how CNCs and PBS work together to affect PLA. Would there be a synergistic effect (Yang et al., 2013) or an interference (Mao et al., 2016) of the two materials on PLA in the PLA/PBS/CNC composite? The ternary system is entirely biodegradable and is promising in the application of environmental protection and renewable resources. Luzi and coworkers (Luzi et al., 2016) found an improvement in the barrier properties due to the combined nucleation effect of CNCs and PBS in the PLA matrix with the PBS content predetermined to be 20%. Zhang's group (Zhang, & Zhang, 2016) grafted CNCs to PBS and investigated their

* Corresponding author at: College of Science, China University of Petroleum, Beijing 102249, China.
E-mail address: xiaocan.zhang@cup.edu.cn (X. Zhang).

http://dx.doi.org/10.1016/j.carbpol.2017.09.077
Received 24 July 2017; Received in revised form 19 September 2017; Accepted 25 September 2017
Available online 25 September 2017
0144-8617/ © 2017 Elsevier Ltd. All rights reserved.

toughening effect in the PBS/PLA blend, and found that the impact strength and moduli were both increased.

In this work, PLA/CNC, PBS/CNC and PLA/PBS/CNC composite films were prepared by the solution-cast method and the crystallization behavior of PLA was evaluated by DSC. Further, FTIR, contact-angle measurements and dissolution experiments were successively employed to characterize the interfacial interactions in the binary and ternary systems. To the best of our knowledge, this is the first time interfacial affinity has been used to systematically investigate how CNCs and PBS function together to affect the crystallization of PLA. This work will advance our understanding and promote the development of multi-component materials when exploring CNCs.

2. Experimental

2.1. Materials

Commercially available PLLA with the trade name 4032D was supplied by NatureWorks® LLC, USA. The number-average molecular weight (M_n) and the polydispersity index (PDI) were 1.34×10^5 g/mol and 1.86, respectively. Poly(butylene succinate) (PBS) was provided by Xinjiang Lanshan Tunhe Polyester Co., Ltd., China. The intrinsic viscosity of PBS was 1.11 dL $\cdot g^{-1}$ in phenol and 1,1,2,2-tetrachloroethane (50:50 w/w) mixed solvent at 25 °C. The melting temperature of PBS is 115.6 °C. Microcrystalline cellulose (MCC) and dimethylformamide (DMF) were purchased from Tianjin Guangfu Fine Chemical Research Institute. The granularity of MCC was reported in the range of 20–100 μm. Sulfuric acid (H_2SO_4), chloroform ($CHCl_3$), tetrahydrofuran (THF) and other analytical-grade reagents were purchased from Beijing Chemical Plant.

2.2. Extraction of cellulose nanocrystals

CNCs were prepared by H_2SO_4 hydrolysis of MCC. First, 3 g MCC was mixed with 60 wt% H_2SO_4 aqueous solution (45 ml) and then stirred vigorously at 50 °C for 2 h. A ten-fold volume of deionized water was then applied to stop the hydrolysis reaction. The solution was left undisturbed for a day, and the resultant suspension was centrifuged at 10^4 r/min for 10 min to separate the crystals, which were subsequently washed with distilled water. The centrifugation process was repeated three times before dialysis was performed overnight against distilled water to reach approximate neutrality. Finally, CNCs in the form of loose powder were obtained after freeze–drying.

2.3. Preparation of composite materials

PLA/CNC, PBS/CNC and PLA/PBS/CNC composite films were prepared by a solvent casting method. The content of CNCs was kept at 3 wt%, and the ratios of the polymers varied. The weighed polymers (1 g) were dissolved in 25 mL DMF with vigorous stirring at 70 °C for 12 h. The dissolved solution was then poured onto a 9–cm diameter Petri dish and heated at 70 °C for 4 h. All samples were subsequently placed in a vacuum oven at 40 °C for 12 h in order to remove the residual solvent.

2.4. Characterizations

2.4.1. Wide angle X-ray diffraction analysis (WAXD)

WAXD measurements were performed on a Bruker AXS D8 instrument using a graphite-filtered *Cu* K_α radiation target ($\lambda = 0.154$ nm) at ambient conditions. Data were collected in the 2θ interval from 5° to 40° with a scan rate of 2°/min.

2.4.2. Transmission electron microscopy (TEM)

TEM observation of CNCs was carried out on an FEI F20 transmission electron microscope. A mass of 10 mg of CNCs was well dispersed in 10 ml of distilled water for 30 min with ultrasonic treatment.

2.4.3. Fourier transform infrared (FTIR) spectroscopy

FTIR spectra of the powdered CNCs, as well as the nanocomposite sheets, were recorded on a Bruker Tensor II spectrometer under the ATR mode by signal averaging over 32 scans at a resolution of 4 cm^{-1}. The powder samples were analyzed using a KBr-pellet method.

2.4.4. Differential scanning calorimetry analysis (DSC)

Thermal analysis of the samples was conducted using DSC (204 F1, NETZSCH) under argon atmosphere. For non-isothermal melt crystallization, the samples were heated from 25 to 195 °C, held isothermally for 5 min to remove thermal history, and then cooled to 25 °C. The heating and cooling rates were 10 °C/min and 5 °C/min, respectively. For isothermal melt crystallization, the samples were heated from 25 to 195 °C, held isothermally for 5 min to remove thermal history, and then quench-cooled to 126 °C.

2.4.5. Contact-angle (CA) measurements

The interfacial tensions between the components in the composites were determined using a CA instrument (DCAT21, Dataphisca, Germany) at 20 °C. Before measurement, films of pure PLA and pure PBS were prepared through compression molding at 195 °C. Measurement of a given contact angle was carried out at least five times and the values were averaged. Double-distilled water and ethylene glycol were used as probe liquids.

3. Results and discussion

3.1. Characterizations of CNC

Sulfuric acid has been used extensively for decades to hydrolyze cellulose (Marchessault, Morehead, & Walter, 1959). Upon hydrolysis, the amorphous regions of MCC were preferentially reacted while the crystalline regions remained intact. The WAXD pattern of the CNCs is shown in Fig. 1A. The diffraction peaks of the 2θ angles at approximately 14.8°, 16.6°, 22.3° and 34.4° are consistent with what has been reported (Cao, Habibi, & Lucia, 2009; Jonoobi, Mathew, Abdi, Makinejad, & Oksman 2012; Lin, Huang, Chang, Feng, & Yu, 2011; Tingaut, Zimmermann, & Lopez-Suevos, 2010). The degree of crystallinity of CNC was calculated (Park, Baker, Himmel, Parilla, & Johnson, 2010) to be 75%

TEM was used to examine the morphology and the rod-like structure of CNCs and the results are shown in Fig. 1B. CNCs possessed a diameter of 10–20 nm with their length in the range of 70–300 nm. The large distribution range in size was expected, due to the diffusion-controlled nature (Cao, Habibi, & Lucia, 2009) upon acid hydrolysis. The chemical structures of CNCs were also analyzed by FTIR and the absorption spectrum is presented in Fig. 1C. The broad band at 3400 cm^{-1} are assigned to the free −OH groups. The vibrations at approximately 2900 cm^{-1} and 1640 cm^{-1} were associated with the stretching of C−H and the absorbed water, respectively. All the characterizations agreed well with literature values (Cao, Habibi, & Lucia, 2009; Jonoobi, Mathew, Abdi, Makinejad, & Oksman 2012; Lin, Huang, Chang, Feng, & Yu, 2011; Tingaut et al., 2010).

3.2. Crystallization behavior

Both non-isothermal and isothermal crystallization behavior was analyzed by DSC. Fig. 2A illustrates the melt-crystallization DSC curves of neat PLA, PLA/CNC, PBS/CNC and PLA/PBS/CNC composites. Neat PLA showed no crystallization on cooling while a crystallization peak appeared at around 116.5 °C with the addition of CNC, and is attributed to the nucleation effect of the addition (Fortunati et al., 2012; Kamal & Khoshkava, 2015). Similarly, the crystallization of PBS was also enhanced by introducing CNC, as evidenced by the increase in T_c

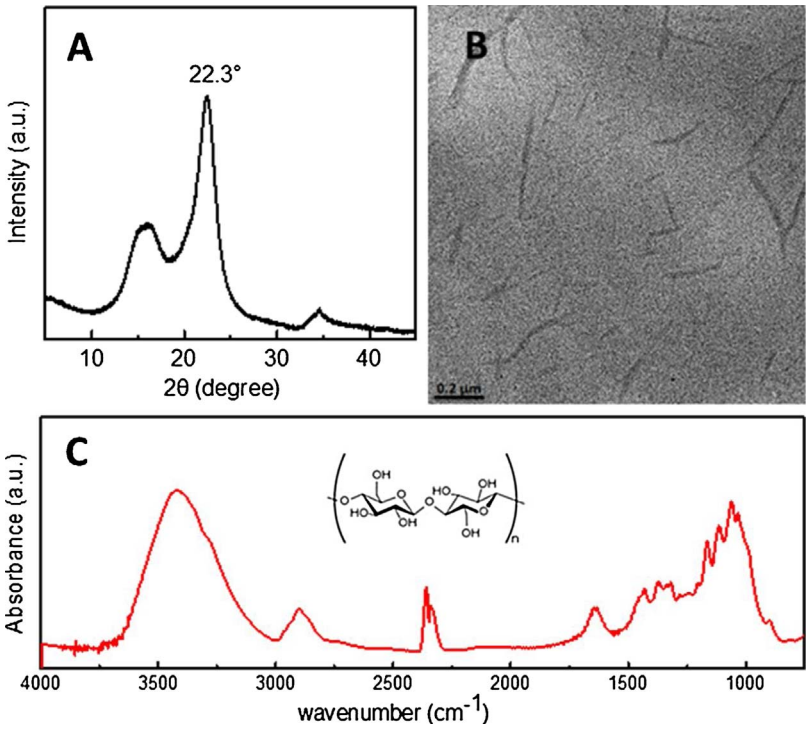

Fig. 1. (A) WAXD patterns, (B) TEM images and (C) FTIR spectra of CNCs.

from 79 °C for neat PBS to 81 °C for the PBS/CNC blend.

Interestingly, no crystallization peaks appeared in the ternary system upon the incorporation of 10% PBS. Here, the enhanced crystallization of PLA by CNC was inhibited by the addition of PBS. It seemed that CNC and PBS interfered for the crystallization enhancement for PLA. Plausibly, PBS separated PLA from CNC, whose nucleation effect was then considerably reduced. Taking the relative amount of the blending components into consideration, this process can be tentatively considered possible by the wrapping of CNCs by PBS. That is to say, the interactions between CNC and PBS might be stronger than those between CNC and PLA. As a result, most of the CNC surfaces would be covered by PBS chains and the heterogeneous nucleation effect of CNC on PLA would therefore be restricted. Similar phenomena were observed in the PVDF/PBS/CNT system (Mao et al., 2016).

Moreover, as shown in Fig. 2A, with higher PBS content (*i.e.*, 20%) in the ternary composite, a new exothermic peak appeared at a temperature of 76 °C, and can be assigned to the crystallization of PBS. In the blend of PLA/PBS (Fig. 2B), PBS did not crystallize in systems where it was present in less than 40 wt%. Comparing these two systems, it is apparent that the crystallization of PBS occurred more readily under these conditions in the ternary composite. This is in keeping with what had been proposed earlier that a stronger interaction existed between CNC and PBS, which restricted the crystallization of PLA. In other words, CNC was thought to be mainly located in PBS rather than in PLA so that only the crystallization of PBS was enhanced.

Isothermal crystallization kinetics of neat PLA and the composites was also studied. Fig. 3 displays the plots of relative crystallinity versus crystallization time and the corresponding Avrami plots for all samples. Fig. 3A demonstrates that the crystallization half-time ($t_{0.5}$) was significantly shortened from 33.7 min for neat PLA to 1.7 min for PLA/CNC composite, and then increased to 10 min in the ternary system with 10% PBS. CNCs had accelerated the overall isothermal melt crystallization of PLA in the binary blend and the prolonged $t_{0.5}$ in the ternary composite can be explained in similar fashion to what had been reported in the non-isothermal section. PBS might strongly interact with CNC and consequently weaken its nucleation effect on PLA.

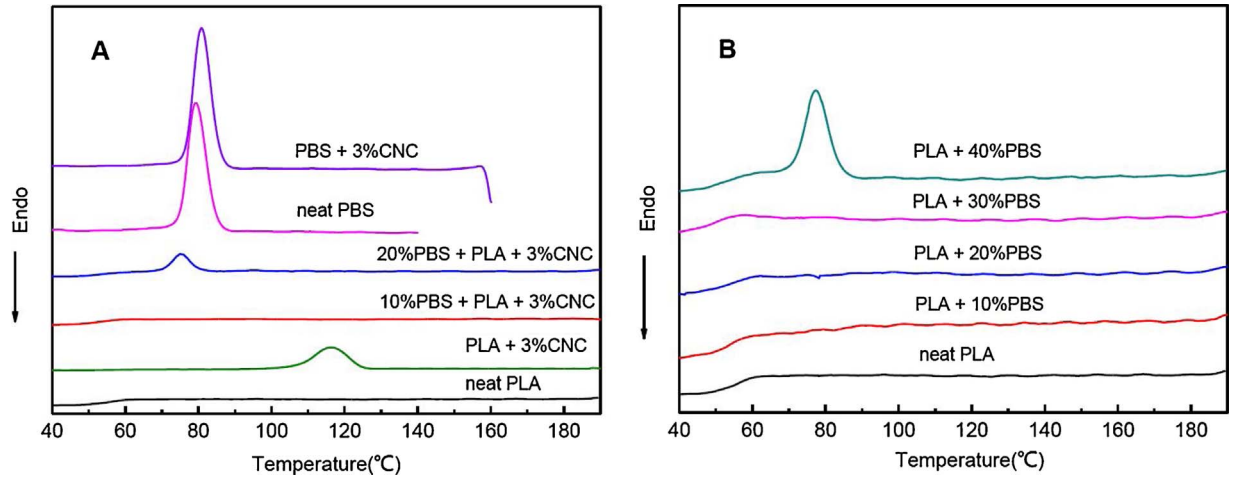

Fig. 2. DSC results for neat PLA and the composites during the first cooling scans.

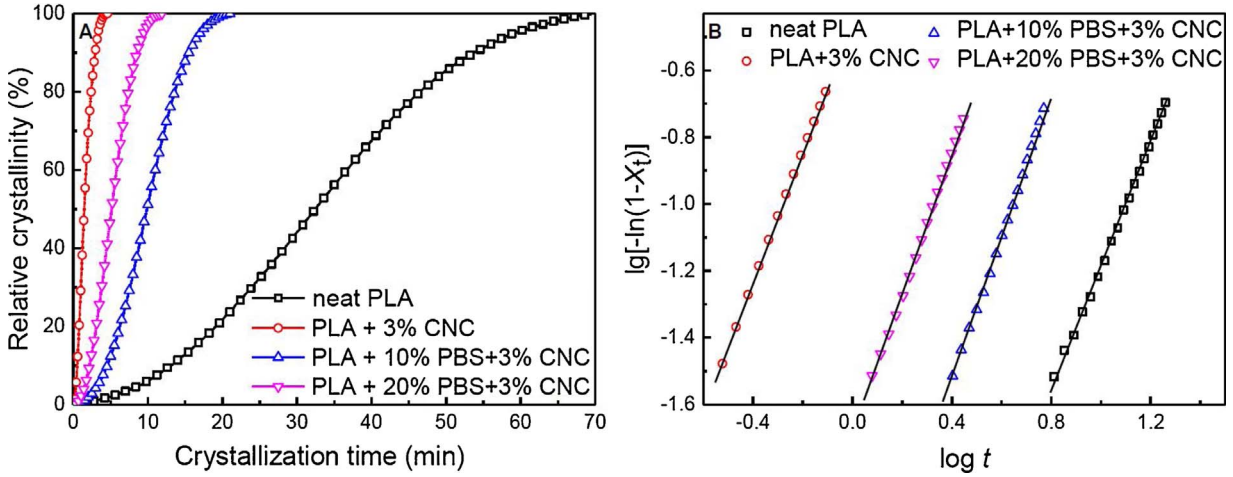

Fig. 3. (A) Plots of relative crystallinity versus crystallization time and (B) the related Avrami plots after isothermally crystallized at 126 °C for neat PLA and the composites.

Further increasing the amount of PBS once again reduced the $t_{0.5}$ to 5.3 min due to its flexible nature and that it functioned as a plasticizer to enhance the mobility of PLA chains (Zhang et al., 2017). The well-known Avrami equation (Song & Qiu, 2009) was also employed to analyze the overall isothermal melt-crystallization kinetics of PLA. The equation is given as:

$$1 - X_t = \exp(-kt^n)$$

where n is the Avrami exponent related to nucleation mechanism (homogeneous or heterogeneous) and growth dimension of crystal, and k is the crystallization rate constant composed of both nucleation and growth parts. Calculated parameters of n, k, and $t_{0.5}$ are summarized in Table 1. The n values vary slightly between 1.8 and 2.2, indicating that the crystallization mechanism remained relatively unchanged for all of the samples and it may be due to a three-dimensional truncated sphere growth (Wunderlich, 1976). The addition of CNCs and PBS did not change the spatial growth behavior of PLA. Nevertheless, the introduction of PBS restricted the crystallization of the composite because $t_{0.5}$ initially increased.

3.3. FTIR test results

It is well known that frequency shifts and intensity changes are characteristic of H–bonds, which would exist in CNC–PBS and CNC–PLA, respectively. For that reason, FTIR analysis was conducted to understand the possible interactions in the composites. In order to intensify the interaction signals among different components, the following actions were performed. Firstly, all specimens with CNCs were extracted with excess chloroform triplicate to remove any free materials. Secondly, the precipitates were centrifuged at 10^4 r/min for 10 min and then vacuum dried at 40 °C for 48 h before FTIR analysis. The amorphous state of the neat materials was used for characterization. Specifically, PLA was prepared by melt-quenching from 195 °C to the room temperature and PBS was examined in the molten state at 140 °C.

Fig. 4 shows the FTIR spectra of the binary and ternary composites as well as the neat polymers. The amorphous PLA exhibited an absorption peak at 1750 cm^{-1}, which is consistent with what had been reported (Urayama, Moon, & Kimura, 2003). Upon the addition of CNCs, the absorption peak appeared at 1759 cm^{-1}, which is characteristic of carbonyl stretching bands attributed to the *gt* conformers (Kister, Cassanas, and Vert, 1998; Sarasua, Rodriguez, Arraiza, & Meaurio, 2005). Likewise, PBS/CNC shows the relative absorbance at 1729 cm^{-1} in reference to the absorbance at 1738 cm^{-1} for neat PBS film that are amorphous in nature (Dong, He, Shin, & Inoue, 2004; Luo et al., 2013). The shift in the peaks can be attributed to the presence of enhanced intermolecular hydrogen bonding between CNCs and the polymer matrix in the binary system. In the PLA/PBS/CNC composite, the carbonyl stretching band at 1759 cm^{-1} disappeared, and only that of PBS at 1729 cm^{-1} remained. This is a clear indication, if not a proof, that the interface interactions between PBS and CNCs were much stronger than those between PLA and CNCs, hence, the surface of CNCs was still covered by notable PBS chains even after extraction.

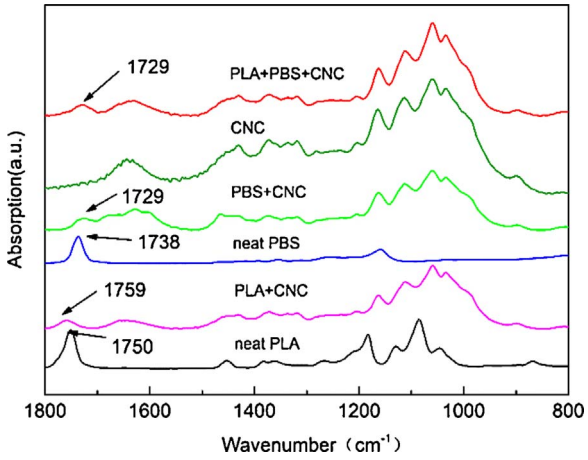

Fig. 4. FTIR spectra of amorphous PLA, amorphous PBS, binary composites PLA/CNC and PBS/CNC, as well as the ternary composite PLA/PBS/CNC.

Table 1
Summary of the overall isothermal melt crystallization kinetics parameters of neat PLA and the composites.

samples	n	k (min^{-n})	$t_{0.5}$ (min)
neat PLA	1.8	8.9×10^{-4}	33.7
3%CNC + PLA	1.9	3.5×10^{-1}	1.7
10%PBS + 3%CNC + PLA	2.2	3.8×10^{-3}	10.0
20%PBS + 3%CNC + PLA	2.1	2.0×10^{-2}	5.3

3.4. Contact-angle measurements

Contact-angle measurements had been conventionally employed to evaluate the surface energy of various materials (Wu, 1982). The involved interfacial tension between fillers and matrix polymers would play a big role in the nucleating activity of the former. It was hence used to compare the interactions between CNC–PBS and CNC–PLA.

Table 2
Surface energy data of the components.

components	γ (mN m^{-1})	γ^d (mN m^{-1})	γ^P (mN m^{-1})
CNC	57.67	7.75	49.92
PBS	30.63	16.44	14.19
PLA	30.28	23.23	7.05

Owens and Wendt (Owens & Wendt, 1969) related surface energy (γ) to the measured contact angle (θ):

$$\gamma_l(1 + cos\theta) = 2(\gamma_s^d \gamma_l^d)^{1/2} + 2(\gamma_s^p \gamma_l^p)^{1/2} \quad (1)$$

where the subscripts l and s denote liquid and solid, respectively. Fowkes (Fowkes, 1962) suggested that the surface free energy of a solid consists of two components, namely, the dispersive component (γ^d) and the polar component (γ^p):

$$\gamma_s = \gamma_s^d + r_s^p \quad (2)$$

Consequently, by measuring the contact angels of the two test liquids and the polar and dispersive components of these two liquids, the surface energy can be calculated. Here, the representative liquids were water and ethylene glycol, and the corresponding parameters $\gamma^p = 51$ mJ m^{-2} and $\gamma^d = 21.8$ mJ m^{-2} for H_2O, $\gamma^p = 19$ mJ m^{-2} and $\gamma^d = 29$ mJ m^{-2} for glycol were used (Liu & Wang, 2010; Yan et al., 2005). The contact angles of water and glycol on different surfaces were 42° and 26° for CNCs, 75° and 54° for PBS and 82° and 56° for PLA, respectively. Based on the aforementioned parameters, the surface energy data of the components were calculated and listed in Table 2.

Furthermore, the interfacial energy can be calculated according to the harmonic mean equation or the geometric mean equation (Wu, 1982):

$$\gamma_{12} = \gamma_1 + \gamma_2 - 4\left(\frac{\gamma_1^d \gamma_2^d}{\gamma_1^d + \gamma_2^d} + \frac{\gamma_1^p \gamma_2^p}{\gamma_1^p + \gamma_2^p}\right) \quad (3)$$

$$\gamma_{12} = \gamma_1 + \gamma_2 - 2(\sqrt{\gamma_1^d \gamma_2^d} + \sqrt{\gamma_1^p \gamma_2^p}) \quad (4)$$

The values of interfacial tensions obtained from Eqs. (3) and (4) are 23.0 mJ m^{-2} and 12.5 mJ m^{-2} for CNC–PBS and 40.0 mJ m^{-2} and 23.6 mJ m^{-2} for CNC–PLA, respectively. These results clearly demonstrate that the CNC–PBS interface had a weaker interfacial tension than that in CNC–PLA. As a result, a stronger interaction (*i.e.*, interfacial affinity) exist between CNCs and PBS, and these results are consistent with the previous discussion.

3.5. Dissolution experiments

In the above sections, the addition of 10% PBS in the PLA/CNC blend was shown to weaken the crystallization of PLA. It had been speculated that the interactions among interfaces in the ternary composite caused the change. FTIR and contact-angle measurements suggested that the interfacial affinity between CNC–PBS was higher than that in CNC–PLA. If this were true, CNCs and PBS would be more difficult to separate than CNCs and PLA. In this regard, a set of dissolution experiments were designed and carried out.

As shown in the flow chart in Fig. 5, all three ingredients were precisely weighted (2.7 *g* PLA, 0.3 *g* PBS and 0.1 *g* CNCs) and the polymer composite film was prepared in the same way as before. The film was immersed in THF at 50 °C for 12 h to ensure complete dissolution of PLA. It was seen that the resultant materials exhibited dissimilar features, namely, the cloudy suspended substance and the bulk sediment. Subsequently, the suspension and the sediment were separately collected and dried at 50 °C overnight. They weighed 0.082 *g* and 0.311 *g*, respectively, suggesting the complete removal of PLA.

The suspension could be either the CNCs originally dispersed in PLA or the pieces of PBS/CNC complexes. In order to confirm the exact

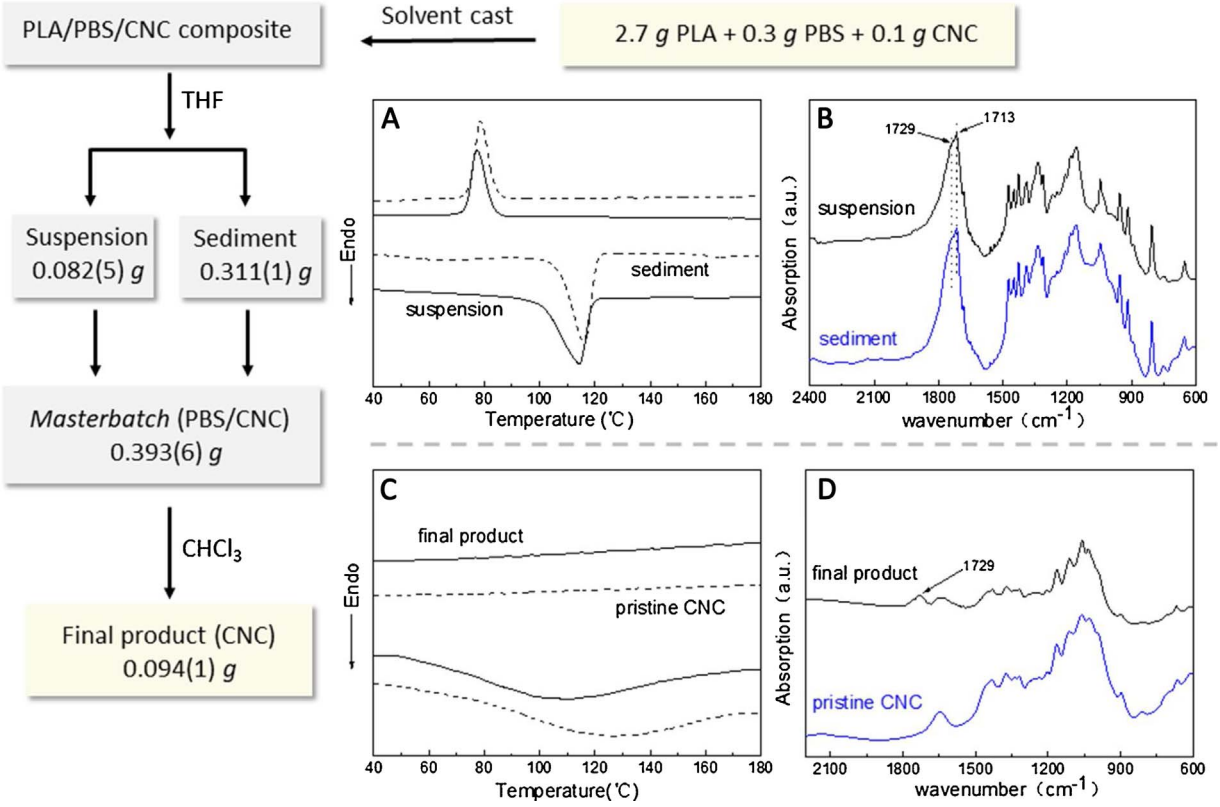

Fig. 5. Flow chart showing the procedures of the dissolution experimentation with characterizations of the intermediates and the final product.

composition of these intermediates, DSC and FTIR were conducted and shown in Fig. 5A and B. Notably, both the suspension and the sediment displayed a T_m of 114 °C, in accordance with the T_m of PBS. In addition, their FTIR results showed absorption peaks at 1729 cm^{-1} and 1713 cm^{-1}, which are the carbonyl stretching bands of PBS with different conformations (Dong, He, Shin & Inoue, 2004). Therefore, it can be concluded that the suspension and the sediment were the same in nature and they were PBS/CNC complexes. They were then combined as 'masterbatch' for further use.

Next, the preceded masterbatch was extracted with excess of chloroform to dissolve PBS, and the detailed procedure was the same as that described in Section 3.3. DSC and FTIR (Fig. 5C and D) were carried out to compare the final product and pristine CNC. DSC results exhibited neither the T_m of PLA nor PBS, suggesting that only CNCs remained during the second dissolution experiment. In the FTIR spectra, the extracted sample had an additional peak at 1729 cm^{-1}, corresponding to the shifted carbonyl group in PBS. The remaining amount of PBS was trivial so that it was not picked up by DSC. The results indicated that the final product was primarily CNCs and that the interactions between PBS and CNCs were rather strong. In addition, the final product weight 0.094 g, approaching to the original 0.1 g for CNCs. It denoted that CNCs indeed almost exclusively located in the PBS component rather than PLA. In all, the above dissolution experiments proved that CNCs had a much stronger interaction with PBS than PLA in the ternary composite, therefore, CNCs were predominantly dispersed in the PBS regions.

4. Conclusions

In this article, CNCs were introduced to PLA, PBS and PLA/PBS composites and their respective crystallization behavior was studied. CNCs were good nucleation agent for individual PLA and PBS as their crystallization peak appeared and had a 2 °C increase, respectively. It was interesting to find that the enhanced crystallization of PLA by CNCs was disappeared in the ternary system.

Isothermal crystallization experiments revealed that the crystallization mechanism remained unchanged. FTIR, contact-angle measurements and the dissolution experiments proved that interfacial affinity between PBS and CNCs was greater than that between PLA and CNCs. Hence, PBS segments tend to occupy most of the CNC surfaces in the molten state, and crystallize in PLA/PBS/CNC composite. On the other hand, the PLA segments were blocked from the CNCs to a large extend and its crystallization was greatly reduced. The results can be further considered for the design and selections of nucleation agents in multicomponent material combinations.

Acknowledgements

We thank Professor Kathy L. Singfield from Saint Mary's University for English editing. This work is partially supported by the Scientific Research Foundation for the Returned Overseas Chinese Scholars, State Education Ministry.

References

Auras, R., Harte, B., & Selke, S. (2004). An overview of polylactides as packaing materials. *Macromolecular Bioscience, 4*(9), 835–864.
Barrau, S., Vanmansart, C., Moreau, M., Addad, A., Stoclet, G., Lefebvre, J. M., et al. (2011). Crystallization behavior of carbon nanotube-polylactide nanocomposites. *Macromolecules, 44*(16), 6496–6502.
Cao, X., Habibi, Y., & Lucia, L. A. (2009). One-pot polymerization, surface grafting, and processing of waterborne polyurethane-cellulose nanocrystal nanocomposites. *Journal of Materials Chemistry, 19*, 7137–7145.
Chen, G. Q., & Patel, M. K. (2011). Plastics derived from biological sources: Present and future: A technical and environmental review. *Chemical Reviews, 112*(4), 2082–2099.
Dong, T., He, Y., Shin, K., & Inoue, Y. (2004). Formation and characterization of inclusion complexes of poly(butylene succinate) with alpha- and gamma-cyclodextrins. *Macromolecular Bioscience, 4*(12), 1084–1091.
Fortunati, E., Peltzer, M., Armentano, I., Torre, L., Jiménez, A., & Kenny, J. M. (2012). Effects of modified cellulose nanocrystals on the barrier and migration properties of PLA nano-biocomposites. *Carbohydrate Polymers, 90*, 948–956.
Fowkes, F. M. (1962). Determination of interfacial tensions, contact angles, and dispersion forces in surfaces by assuming additivity of intermolecular interactions in surfaces. *Journal of Physical Chemistry, 66*, 382–389.
Habibi, Y., Lucia, L. A., & Rojas, O. J. (2010). Cellulose nanocrystals: Chemistry, self-assembly, and applications. *Chemical Reviews, 110*(6), 3479–3500.
Harris, A. M., & Lee, E. C. (2008). Improving mechanical performance of injection molded PLA by controlling crystallinity. *Journal of Applied Polymer Science, 107*(4), 2246–2255.
Hu, F., Lin, N., Chang, P. R., & Huang, J. (2015). Reinforcement and nucleation of acetylated cellulose nanocrystals in foamed polyester composites. *Carbohydrate Polymers, 129*, 208–215.
Jonoobi, M., Mathew, A. P., Abdi, M. M., Makinejad, M. D., & Oksman, K. (2012). A comparison of modified and unmodified cellulose nanofiber reinforced polylactic acid (PLA) prepared by twin screw extrusion. *Journal of Polymers and the Environment, 20*, 991–997.
Kamal, M. R., & Khoshkava, V. (2015). Effect of cellulose nanocrystals (CNC) on rheological and mechanical properties and crystallization behavior of PLA/CNC nanocomposites. *Carbohydrate Polymers, 123*, 105–114.
Kister, G., Cassanas, G., & Vert, M. (1998). Effects of morphology, conformation and configuration on the IR and Raman spectra of various poly(lactic acid)s. *Polymer, 39*(2), 267–273.
Lin, N., Huang, J., Chang, P. R., Feng, J., & Yu, J. (2011). Surface acetylation of cellulose nanocrystal and its reinforcing function in poly (lactic acid). *Carbohydrate Polymers, 83*(4), 1834–1842.
Lin, N., Chen, Y., Hu, F., & Huang, J. (2015). Mechanical reinforcement of cellulose nanocrystals on biodegradable microcellular foams with melt-compounding process. *Cellulose, 22*(4), 2629–2639.
Liu, Z., & Wang, J. (2010). Preparation of Maleic Anhydride-g-liquid Polybutadiene Grafting siloxane and study on its surface free energy. *Silicone Material, 24*, 351–355.
Lizundia, E., Vilas, J. L., & León, L. M. (2015). Crystallization, structural relaxation and thermal degradation in poly (l-lactide)/cellulose nanocrystal renewable nanocomposites. *Carbohydrate Polymers, 123*, 256–265.
Lizundia, E., Fortunati, E., Dominici, F., Vilas, J. L., León, L. M., Armentano, I., et al. (2016). PLLA-grafted cellulose nanocrystals: Role of the CNC content and grafting on the PLA bionanocomposite film properties. *Carbohydrate Polymers, 142*, 105–113.
Luo, F. L., Luo, F. H., Xing, Q., Zhang, X. Q., Jiao, H. Q., Yao, M., et al. (2013). Hydrogen-bonding induced change of crystallization behavior of poly(butylene succinate) in its mixtures with bisphenol A. *Chinese Journal of Polymer Science, 31*(12), 1685–1696.
Luzi, F., Fortunati, E., Jiménez, A., Puglia, D., Pezzolla, D., Gigliotti, G., et al. (2016). Production and characterization of PLA_PBS biodegradable blends reinforced with cellulose nanocrystals extracted from hemp fibres. *Industrial Crops and Products, 93*, 276–289.
Mao, H., Zhang, T., Zhang, N., Huang, T., Yang, J., & Wang, Y. (2016). Largely restricted nucleation effect of carbon nanotubes in a miscible poly (vinylidene fluoride)/poly (butylene succinate) blend. *Polymer International, 65*(12), 1417–1429.
Marchessault, R. H., Morehead, F. F., & Walter, N. M. (1959). Liquid crystal systems from fibrillar polysaccharides. *Nature, 184*, 632–633.
Owens, D. K., & Wendt, R. C. (1969). Estimation of surface free energy of polymers. *Journal of Applied Polymer Science, 13*, 1741–1747.
Pan, H., & Qiu, Z. (2010). Biodegradable poly (*l*-lactide)/polyhedral oligomeric silsesquioxanes nanocomposites: Enhanced crystallization, mechanical properties, and hydrolytic degradation. *Macromolecules, 43*(3), 1499–1506.
Park, J. W., & Im, S. S. (2002). Phase behavior and morphology in blends of poly(L-lactic acid) and poly(butylene succinate). *Journal of Applied Polymer Science, 86*(3), 647–655.
Park, S., Baker, J. O., Himmel, M. E., Parilla, P. A., & Johnson, D. K. (2010). Cellulose crystallinity index: Measurement techniques and their impact on interpreting cellulase performance. *Biotechnology for Biofuels, 3*(1), 1–10.
Park, S. B., Hwang, S. Y., Moon, C. W., Im, S. S., & Yoo, E. S. (2010). Plasticizer effect of novel PBS ionomer in PLA/PBS ionomer blends. *Macromolecular Research, 18*(5), 463–471.
Saeidlou, S., Huneault, M. A., Li, H., & Park, C. B. (2012). Poly (lactic acid) crystallization. *Progress in Polymer Science, 37*(12), 1657–1677.
Sarasua, J. R., Rodriguez, N. L., Arraiza, A. L., & Meaurio, E. (2005). Stereoselective crystallization and specific interactions in polylactides. *Macromolecules, 38*, 8362–8371.
Shibata, M., Inoue, Y., & Miyoshi, M. (2006). Mechanical properties, morphology, and crystallization behavior of blends of poly(L-lactide) with poly(butylene succinate-co-L-lactate) and poly (butylene succinate). *Polymer, 47*(10), 3557–3564.
Sinba, R. S. (2012). Polylactide-based bionanocomposites: A promising class of hybrid materials. *Accounts of Chemical Research, 45*(10), 1710–1720.
Song, L., & Qiu, Z. (2009). Crystallization behavior and thermal property of biodegradable poly (butylenesuccinate)/functional multi-walled carbon nanotubes nanocomposite. *Polymer Degradation and Stability, 94*, 632–637.
Tingaut, P., Zimmermann, T., & Lopez-Suevos, F. (2010). Synthesis and characterization of bionanocomposites with tunable properties from poly(lactic acid) and acetylated microfibrillated cellulose. *Biomacromolecules, 11*, 454–464.
Urayama, H., Moon, S., & Kimura, Y. (2003). Microstructure and thermal properties of polylactides with different l - and d -Unit sequences: Importance of the helical nature of the L-sequenced segments. *Macromolecular Materials and Engineering, 288*, 137–143.
Wu, S. (1982). *Polymer interface and adhesion.* New York: Marcel Dekker.
Wunderlich, B. (1976). *Macromelecular physics.* New York: Academic Press.
Yan, X. B., Xu, T., Yue, S. S., Liu, H. W., Xue, Q. J., & Yang, S. R. (2005). Water-repellency

and surface free energy of a-C:H films prepared by heat-treatment of polymer precursor. *Diamond and Related Materials, 14*, 1342–1347.
Yang, J. H., Shen, Y., He, W. D., Zhang, N., Huang, T., Zhang, J. H., et al. (2013). Synergistic effect of poly (ethylene glycol) and graphene oxides on the crystallization behavior of poly (l-lactide). *Journal of Applied Polymer Science, 130*(5), 3498–3508.
Ye, H., Hou, K., & Zhou, Q. (2016). Improve the thermal and mechanical properties of poly (l-lactide) by forming nanocomposites with pristine vermiculite. *Chinese Journal of Polymer Science, 34*(1), 1–12.
Yokohara, T., & Yamaguchi, M. (2008). Structure and properties for biomass-based polyester blends of PLA and PBS. *European Polymer Journal, 44*(3), 677–685.
Yu, F., Liu, T., Zhao, X., Lu, A., & Wang, J. (2012). Effects of talc on the mechanical and thermal properties of polylactide. *Journal of Applied Polymer Science, 125*(S2), E99–E109.
Zhang, X., & Zhang, Y. (2016). Reinforcement effect of poly(butylene succinate) (PBS)-grafted cellulose nanocrystal on toughened PBS/polylactic acid blends. *Carbohydrate Polymers, 140*, 374–382.
Zhang, X., Liu, Q., Shi, J., Ye, H., & Zhou, Q. (2017). Distinctive tensile properties of the blends of poly(l-lactic acid) (PLLA) and poly(butylene succinate) (PBS). *Journal of Polymers and the Environment*. http://dx.doi.org/10.1007/s10924-017-1064-8.
Zhao, Y., & Qiu, Z. (2015). Effect of poly(vinyl alcohol) as an efficient crystallization-assisting agent on the enhanced crystallization rate of biodegradable poly(L-lactide). *RSC Advance, 5*(61), 49216–49223.